Panel Method for Counter-Rotating Propfans

Shih H. Chen*
Rockwell International, Canoga Park, California 91303
and
Marc H. Williams†
Purdue University, West Lafayette, Indiana 47907

A time-domain source-doublet surface-paneling method is developed for analyzing the unsteady loads on counter-rotating propellers in incompressible irrotational flow. A scheme for treating the blade-wake interaction problem is described. Sample results for single rotation propellers are given with comparisons to alternate theories and experiment. Finally, results for quasisteady and fully unsteady loads on counter-rotating systems are presented.

Nomenclature

C = chord
C_p = pressure coefficient, $p'/\frac{1}{2}\rho U_\infty^2$
C_P = power coefficient
C_T = thrust coefficient
D = rotor diameter
J = advance ratio, U_∞/nD
N_B = number of blades
n = rotational speed, rps
$\boldsymbol{n}$ = unit outward normal
p' = disturbance pressure
r = blade radius
r_{tip} = blade tip radius
U_b = blade velocity
U_T = local blade velocity relative to freestream
U_∞ = axial freestream velocity
u_n = surface normal velocity
u_T = surface tangential velocity
β = blade setting angle at 3/4 radial location
ΔC_p = difference pressure coefficient
ΔC_P = elemental power coefficient
ΔC_T = elemental thrust coefficient
ρ = density
ϕ = velocity potential
Φ = interrow phase angle

Subscripts
1,F = front rotor
2,R = rear rotor
w = wake

Introduction

COUNTER-ROTATING propellers can be 7–12% more efficient than single roation systems[1,2] as shown in Fig. 1. This gain in efficiency is primarily because the rear rotor can recover part of the swirl energy generated by the front blades, (energy that is lost in single rotation.) The saving in fuel, and in direct operating cost, are significant. However, counter-rotation configurations are also significantly more complex than single rotation, both mechanically and aerodynamically. The flow about a single-rotation propeller can for most purposes be assumed steady in a blade frame. In contrast, the flow near a counter-rotating prop can never be steady. This simple fact leads to concern about noise and aeroelastic response for these designs. It also means that the steady flow analysis methods used for the single-rotation designs must be modified to account for unsteadiness. In this paper we will discuss a numerical method for predicting time-dependent loads on counter-rotating propellers.

Early analytical research on counter-rotating propeller systems was begun in the 1940s, as in Lock,[3] who used strip theory, and Theodorsen,[4] who used vortex theory. Both predicted only the time-averaged loads on the front and rear rows, accounting for the interference between the rows by averaging of the induced velocities. This type of analysis has been modernized by Celestina et al.,[5] who solve the steady Euler equations in a typical passage in both the front and rear rotors using a finite-volume numerical scheme. Interference between rows is done through the circumferentially averaged part of the flowfield. The unsteady fluctuations are not resolved. Colehour et al.[6] present some predictions of counter-rotation propeller performance based on two separate methodologies: a semi-empirical quasisteady strip theory and a coupled Euler and actuator disc model. Whitfield et al.[7] use the same equations (Euler equations) and method (finite volume) as do Celestina et al.[6] for high-speed flow but in a unsteady frame (though only time-averaged performance data was shown). The circumferentially averaged mean flow is not

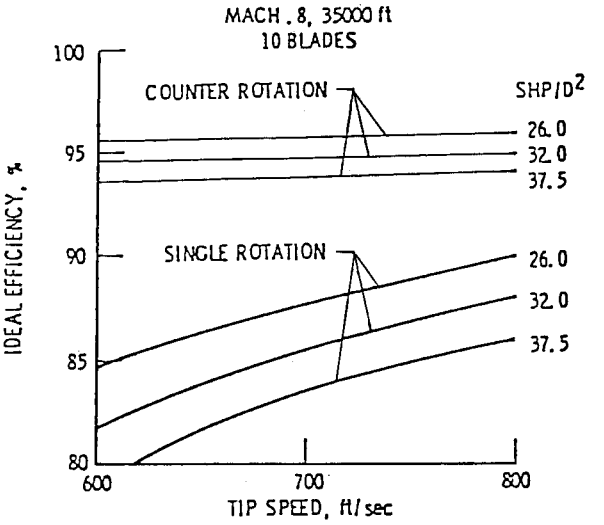

Fig. 1 Comparison of efficiency for single- and counter-rotation propfans.

Presented as Paper 87-1890 at the AIAA/ASME/SAE/ASEE 23rd Joint Propulsion Conference, San Diego, CA, June 29–July 2, 1987. Received Dec. 14, 1989; revision received Sept. 4, 1990; accepted for publication Sept. 24, 1990.

*Member of Technical Staff, Rocketdyne Division.
†Associate Professor, School of Aeronautics and Astronautics.

used in their analysis. Lesieutre and Sullivan[8,9] analyze the counter-rotation problem with a quasisteady three-dimensional vortex lattice model in which the fore and aft blade rows are fully coupled. In this treatment, a sequence of independent calculations are made for various interrow phase angles to construct the quasisteady time history. At each phase angle, the trailing vortices are asasumed to have constant axial strength, which adjusts instantaneously to the current geometry. A two-dimensional Sears gust analysis is then done on each blade, in strip fashion, to account for the presence of the spanwise vorticity that is neglected in the quasisteady analysis. The use of two-dimensional theory to account for the shed vorticity, in effect, assumes that the wavelength is short compared to the span. Since the typical wavelengths are not so short in practice, the accuracy of this model is open to question.

In the present study, as in Lesieutre and Sullivan, the propeller is assumed to operate in an inviscid, incompressible, irrotational flow with a uniform axial speed U_∞ far upstream. The potential field is modeled by source and doublet distributions on the blade and wake surfaces. Such methods have been used by many authors, principally for wing or wing-body configurations in rectilinear motion.[10-13] The present analysis can handle general blade shapes, relative motions, and numbers of blades in the front and rear rows. In this paper, though, we consider only cases in which the blades are all identical (aside from mirror imaging), and the number of blades in the fore and aft rotors is the same. These assumptions permit some reduction in the size of the resulting influence coefficient matrices. In addition, a prescribed rigid wake along the advance ratio was used, (though, again, a more elaborate wake model could be used.) The potential wake assumes vorticity is concentrated in zero thickness sheets and lines. The wakes from the front row diffuse (viscosity) as they convect further downstream. The concentrated vorticity approximation should be satisfactory as long as the spacing between rows is small; it would get worse as the separation increases so the viscous cores are a substantial fraction of a blade chord. The primary distinction between the present method and that of Lesieutre and Sullivan is that we retain both chordwise and spanwise vorticity in the wakes.

The compressibility effect for a realistic propfan operating condition could be included by accounting for acoustic time lags in influence coefficient calculations. This will be performed in the future studies.

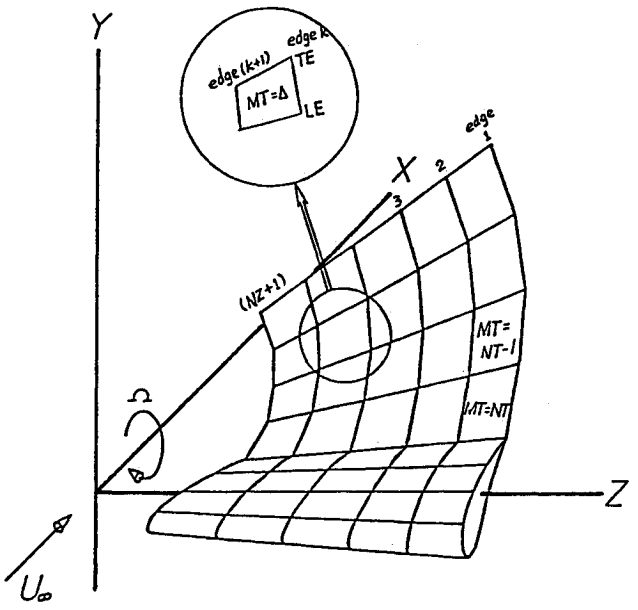

Fig. 2 Blade and wake paneling.

Formulation

We adopt an inertial Cartesian coordinate system X-Y-Z with origin fixed at the center of the front rotor, where X is measured along the downstream axis of rotation (see Fig. 2). Under the stated assumptions, the flowfield is determined by a perturbation velocity potential ϕ, which satisfies Laplace's equation and vanishes at infinity, and a perturbation pressure p', which is obtained from Bernoulli's equation. Using Green's theorem, the potential field at any instant in time, and any field point x, can be expressed as a distribution of sources and doublets over the boundary surface S, which includes all blades and their wakes:

$$4\pi E\phi(x,t) = -\int\int_S \frac{u_n}{R}\,dA_0 + \int\int_S \phi\,\frac{\partial}{\partial n}\left(\frac{1}{R}\right)dA_0$$

$$R = |x - x_0|,\ x_0 \text{ on } S$$

$$E = \begin{cases} 0 & \text{if } x \text{ inside } S \\ \frac{1}{2} & \text{if } x \text{ on } S \\ 1 & \text{if } x \text{ outside } S \end{cases} \tag{1}$$

The first term on the right-hand side of Eq. (1) represents the source distribution, which is known from the flow tangency boundary condition on solid surfaces. The second term on the right-hand side represents the unknown doublet distribution. When specialized to the blade surfaces, Eq. (1) amounts to a Fredholm integral equation of the second kind, which must be solved for the potential distribution on the surface.

Since we are dealing with a perturbation potential, the normal velocity u_n appearing in the source term is given by

$$u_n = \boldsymbol{n} \cdot \boldsymbol{U}_r = (\boldsymbol{U}_b - \boldsymbol{U}_\infty) \cdot \boldsymbol{n} \tag{2}$$

where $\boldsymbol{U}_r$ is the local blade velocity relative to the freestream and $\boldsymbol{n}$ is the unit outward normal to the surface. It should be noted that the blades are not assumed to be rigid. Blade vibration can be included simply by using the correct normal velocity in the source term (with or without altering the blade coordinates, which would only be necessary for very large amplitude vibrations).

Once the surface potentials have been found, the surface pressures can be obtained from Bernoulli's equation, which, on a moving surface, is,

$$\frac{p'}{\rho} = -\frac{\partial\phi}{\partial t} + \frac{1}{2}u_n^2 - \boldsymbol{U}_r \cdot \boldsymbol{u}_T - \frac{1}{2}|\boldsymbol{u}_T|^2$$

$$\boldsymbol{u}_T = \nabla\phi - \boldsymbol{n}u_n \tag{3}$$

In this form, the time derivative is done at a point that is fixed on a blade. Since the normal velocity is specified on the surface, we need only calculate the tangential derivatives of potential to evaluate the pressure.

The wakes are modeled as infinitesimally thin rigid helical surfaces emanating from the blade trailing edges. Therefore, the source terms in Eq. (1) vanish on the wakes, and the doublet terms are determined simply from the potential jump $\Delta\phi_w$ across the wake sheet. The jump is simply convected along the wake at the freestream speed, in accord with the physical constraint that there be no pressure difference across the wake. Therefore, at any instant in time, the wake doublet strengths are known, except at the blade trailing edge, where they are fixed by a Kutta condition.

An unavoidable feature of the counter-rotation problem is that a rear rotor blade will periodically cut through the wakes

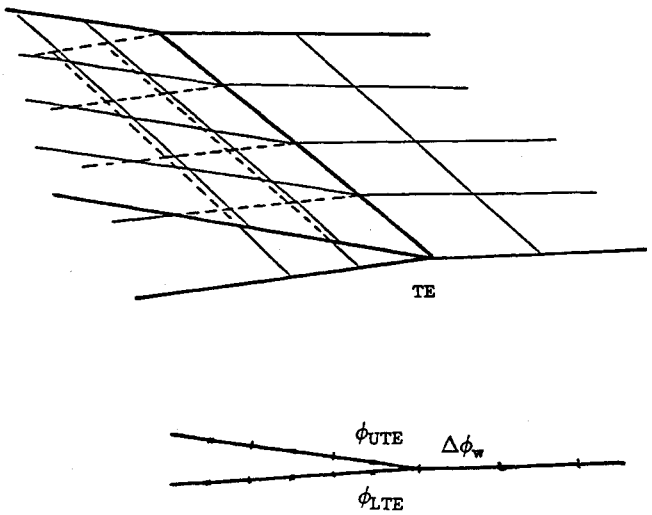

Fig. 3 Blade-wake geometry near trailing edge.

shed by the forward blades. This occurs at multiples of the passing period,

$$T = \frac{1}{(n_1 N_{B_1} + n_2 N_{B_2})} \tag{4}$$

For simplicity, this cutting process is assumed to occur (as in the classical sharp-edged gust problem in linearized aerodynamics) without deformation of the wake outside the passing blade. The segment of wake sheet that would lie within the passing blade is deleted, which is equivalent to merging the wake sheet with the blade surface. Of course, this model implies that the potential distribution on the blade will be discontinuous at the line of intersection between the blade and wake, with jumps equal to the local strength of the wake sheet. After the blade emerges from the wake, the wake sheet is rejoined. This model of wake cutting was chosen because it appears to be the simplest plausible candidate.

Discretization

To obtain an approximate solution of the integral equation, Eq. (1), the blade and wake surfaces are divided into quadrilateral elements, as shown in Fig. 2. The values of ϕ and u_n are treated as constant over each element. The governing equation, Eq. (1), is then imposed at the centroid of each element on the solid surfaces, resulting in a set of simultaneous linear algebraic equations,

$$\begin{aligned} C_{ij}\phi_j &= B_{ij}u_{n_j} - A_{ik}\Delta\phi_{wk} \\ C_{ij} &= \delta_{ij} - \frac{1}{2\pi}\int\int_{S_j} \frac{\partial}{\partial n}\left(\frac{1}{R}\right) \mathrm{d}A_0 \\ B_{ij} &= -\frac{1}{2\pi}\int\int_{S_j} \frac{1}{R}\,\mathrm{d}A_0 \\ A_{ik} &= -\frac{1}{2\pi}\int\int_{S_{wk}} \frac{\partial}{\partial n}\left(\frac{1}{R}\right) \mathrm{d}A_0 \end{aligned} \tag{5}$$

All of the wake doublets are known from the previous time history, except for those at the blade trailing edges. These are treated as unknowns to be determined from the numerical Kutta condition (see Fig. 3),

$$\Delta\phi_w = \phi_{UTE} - \phi_{LTE} \tag{6}$$

The influence coefficients appearing in Eq. (5) depend only on the relative positions of panel and control point. They are computed from a midpoint rule (i.e., point source or dipole) in the far field (more than two panel widths separation) and from the hyperboloidal surface formulas given by Chen et al.[10] in the near field.

The linear algebra problem given in Eq. (5) must be solved at each time step. Note that the influence coefficient matrices corresponding to the interaction of a blade row on itself are independent of time and can be calculated once. The terms corresponding to interaction between blade rows must be updated at each time step. Moreover, if the number of blades in the two rows is the same, as in all the cases considered here, the loads on all blades in a given row will be identical at any given time, so that the order of the problem can be greatly reduced. In that case, one solves only for the doublets on a reference blade in each row, the effects of other blades coming in through the influence coefficient matrices.

When a blade passes through a wake, the paneling procedure described above must be modified to avoid having the wake panel edges (which are singularities) hit the control points on the blade. (If this were to happen, very large disturbances would appear of purely numerical origin.) The procedure that has been used is to keep the blade surface paneling fixed but deform the wake elements in the neighborhood of the blade to match up with the blade panel edges. The line of interaction between the deformed wake and the blade, then, is a zig-zag line following those blade panel edges that lie closest to the true line of intersection between the rigid wake and the blade. Since the difference between the zig-zag and the true line of intersection decreases when the number of panels is increased, the scheme is formally consistent with the mathematical model originally posed. Moreover, a "friendly" distance is always maintained between the edge singularities and the control points, so that unwanted numerical noise is minimized.

Once the surface potentials have been found at a given time, each wake element is convected back at the freestream speed in preparation for the following time step (the doublet strength associated with each wake element is constant while the element moves). The wake element size is found to be optimum if it is of the same order as the blade element size. The axial length of the convected wake is one blade tip diameter or longer to assure steady or periodic response. The surface pressures are obtained directly from Bernoulli's equa-

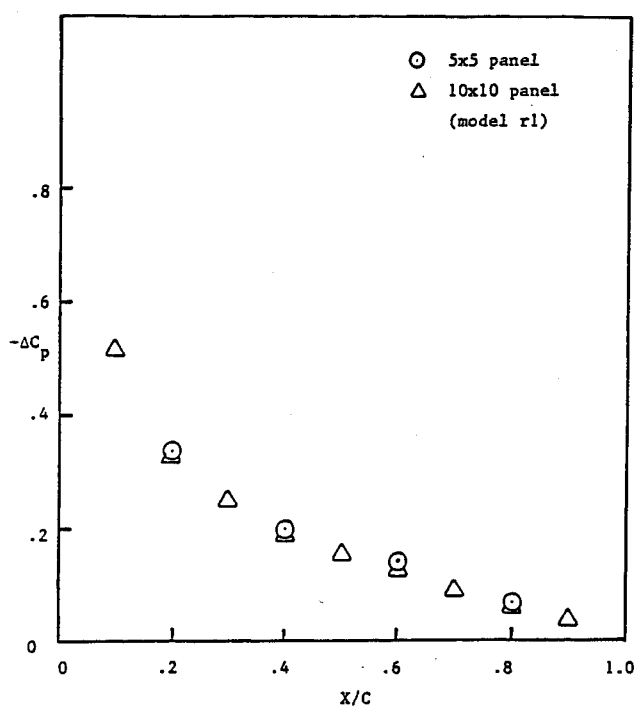

Fig. 4 Convergence test of a thin straight blade (AR = 3.2, t/c = 0.01, r/r_{tip} = 0.92).

tion, Eq. (3), in which the tangential induced velocities are found by finite differences on the surface potential data. The net loads, thrust, and power, for example, are found by simple numerical integration of the pressures over the surface.

Computational Costs

In a typical example of a counter-rotation calculation, with four blades in each row, seven panels on a chord and eight on a span, the blade surfaces are discretized with 896 elements. Counting the 64 Kutta conditions, we have 960 simultaneous equations to be solved at each time step. Using the fact that the number of blades in each row is the same, we can reduce this to 240 equations. The calculation consumes, on a CYBER205, 3.5 minutes for the first time step and 2.5 minutes for subsequent steps (since the diagonal blocks of the influence matrix do not need to be recomputed). The timing ratio using the full matrix and the reduced matrix is approximately $(960/240)^3$. Typically around 20 time steps per passage period are used. No attempt has been made to vectorize the code.

Results

Single Rotation Cases

To test the procedure on simple cases, a number of nonrotating wings and single-rotation propeller examples were examined. Only single-rotating results will be discussed here.

The first test case, shown in Fig. 4, is a straight, moderate aspect ratio blade with a 1% thickness to chord ratio parabolic arc section. This figure shows a comparison between the results of the present scheme for the same case with (5 by 5) and (10 by 10) panels. This indicates that at least for single rotation problems, a fairly small number of panels will suffice.

Figures 5 and 6 are for an eight-bladed rotor of SR2 blades. Comparisons are shown with the lifting surface theory of Ref. (14) for chordwise pressure distribution (Fig. 5), and radial distribution of power (Fig. 6). The agreement between the two calculation methods is generally very good. It should be noted, though, that the present method necessarily uses twice as many panels for the same resolution as the lifting surface method, since both sides of a blade must be paneled.

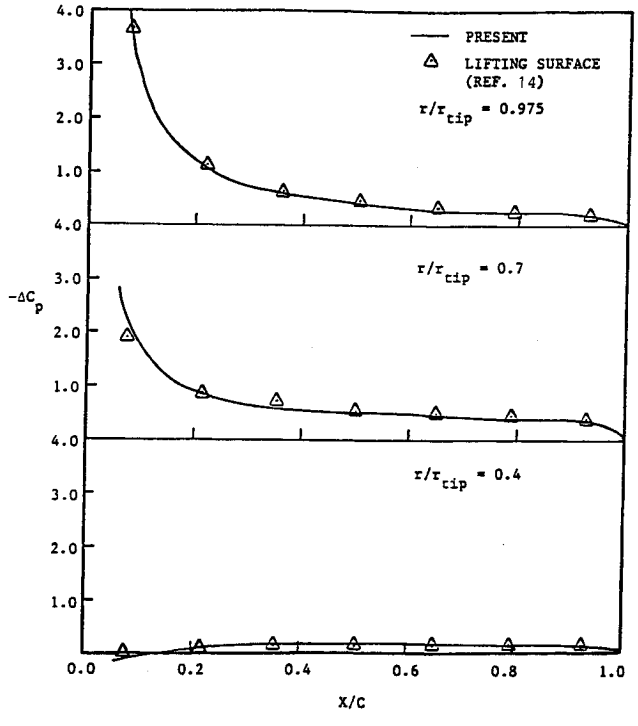

Fig. 5 Pressure distribution on single-rotation SR2 ($\beta_{3/4}$ = 40.3 deg, N_B = 8, J = 1.633).

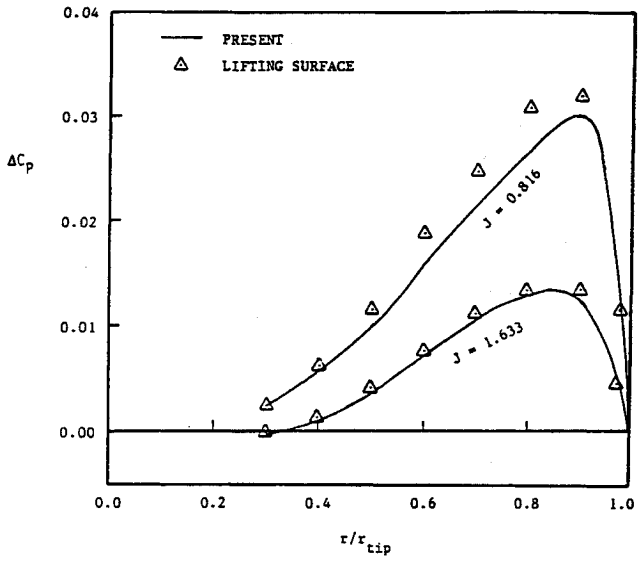

Fig. 6 Power on single-rotation SR2 ($\beta_{3/4}$ = 40.3 deg, N_B = 8).

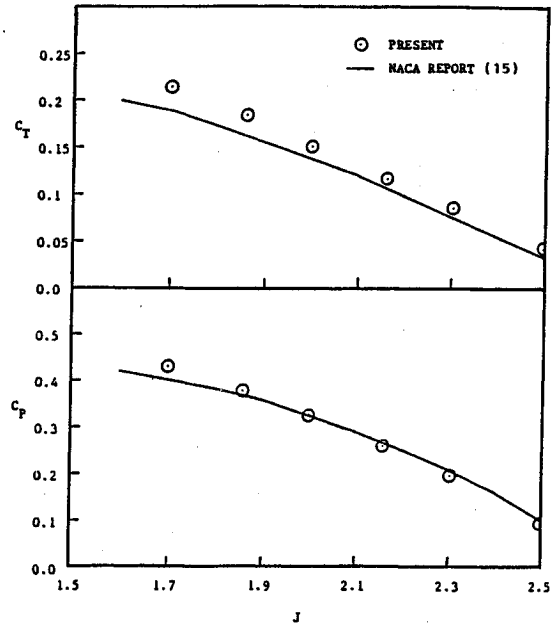

Fig. 7 Comparison of predicted and measured loadings ($\beta_{3/4}$ = 45 deg, N_B = 4, HS3155).

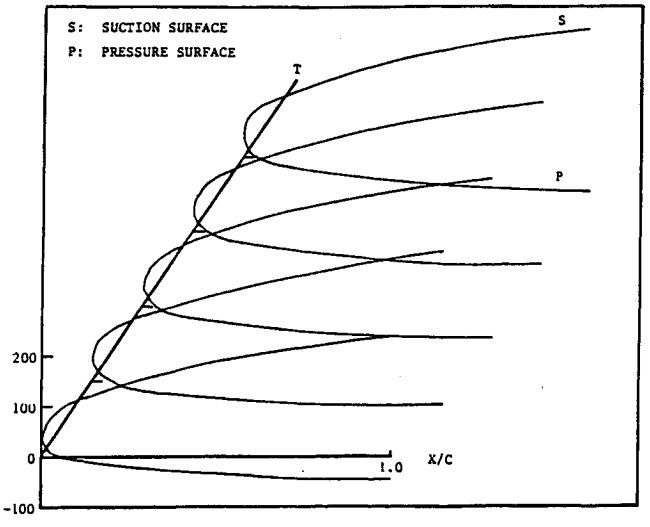

Fig. 8 Time history of velocity potential distribution on front rotor ($\beta_{3/4}$ = 30.45 deg, N_B = 2 × 2, J = 0.816, r/r_{tip} = 0.6, SR2).

As a last example of a single-rotation analysis, we show results for the conventional Hamilton Standard 3155 propeller[15] in Fig. 7. The total thrust and power are in reasonably good agreement with the measured performance characteristics,[15] particularly at low loading. These results are what should be expected from any inviscid rigid wake model.

Counter-Rotation Cases

Two counter-rotating configurations will be discussed, both with four blades in each row, but with different blade geometries. The two blades are the HS3155, a relatively high aspect ratio straight blade, and the SR2, a moderate aspect ratio design.

Since the present method computes surface potentials directly, we begin a discussion of the counter-rotation results by showing computed surface potential distributions, with emphasis on the blade-wake intersection process. While these potential distributions are not of much physical interest, they do demonstrate that the numerical scheme used captures the intended mathematical structure.

In Figs. 8 and 9, we show the potential as a function of chord position and time at 60% of tip radius on the front (Fig. 8) and rear (Fig. 9) blades of a 2-by-2 system of SR2 blades. The potential on the front blade varies smoothly, while that on the rear blade shows a discontinuity propagating from leading edge to trailing edge. This is, of course, the trace of a wake through which the rear blade is passing. An instantaneous picture of the same thing is shown in Fig. 10. The wake spans the entire blade from root to tip. The spanwise variation in the strength of the potential jump mirrors the spanwise circulation distribution on the front blade.

The next case is a 4-by-4 system of HS3155 blades, which has also been studied by Lesieutre et al.[9] The spacing for this

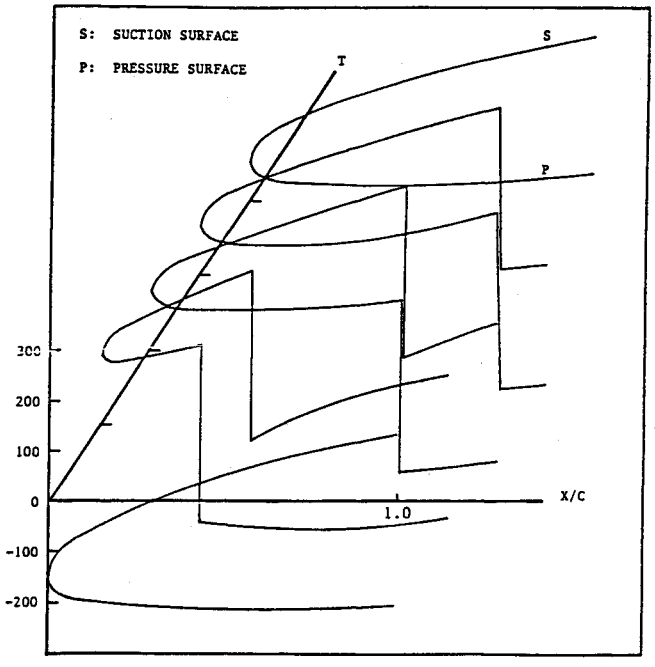

Fig. 9 Time history of velocity potential distribution on rear rotor ($\beta_{3/4}$ = 30.45 deg, N_B = 2 × 2, J = 0.816, r/r_{tip} = 0.6, SR2).

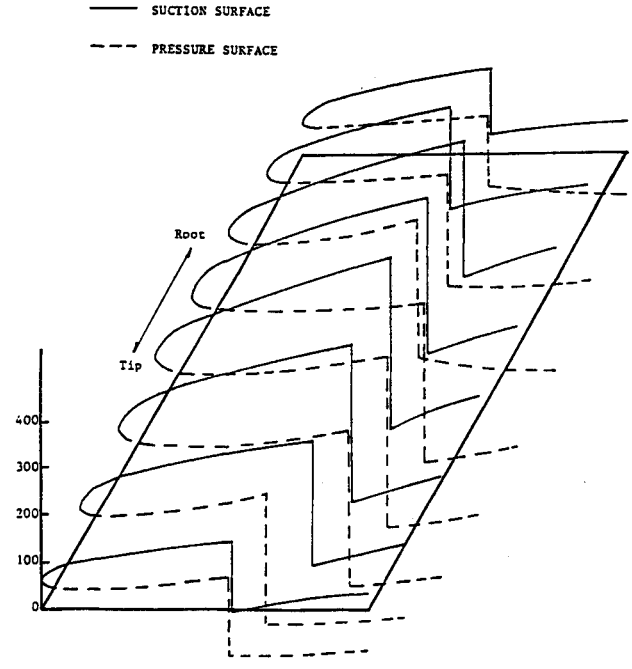

Fig. 10 Rear rotor velocity potential distribution while intersecting wake ($\beta_{3/4}$ = 30.45 deg, N_B = 2 × 2, J = 0.816, r/r_{tip} = 0.6, SR2).

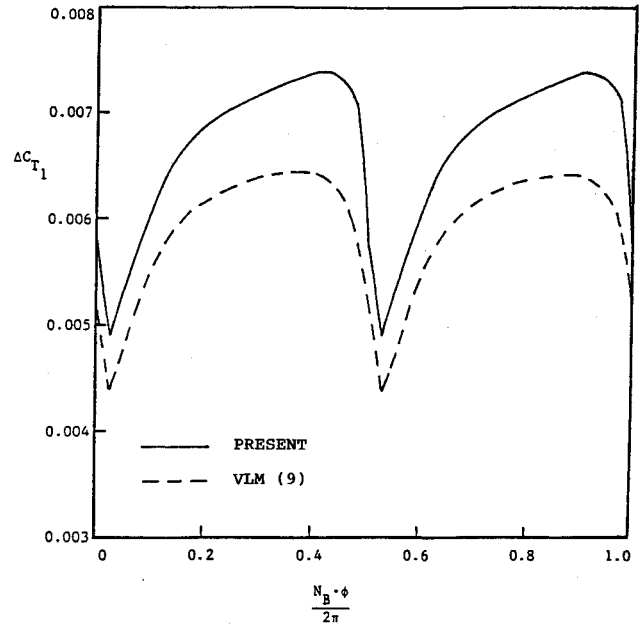

Fig. 11 Quasisteady elemental thrust on front rotor (r/r_{tip} = 0.75, N_B = 4 × 4, β_F = 45 deg, β_R = 44 deg, J = 2.0, HS3155).

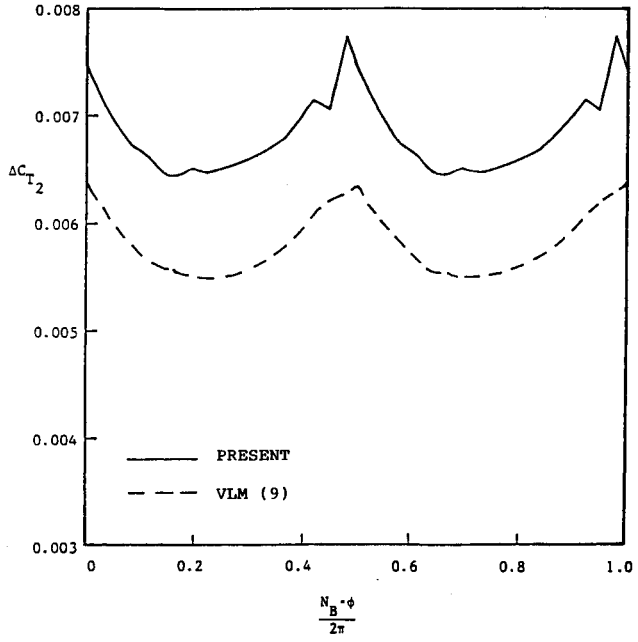

Fig. 12 Quasisteady elemental thrust on rear rotor (r/r_{tip} = 0.75, N_B = 4 × 4, β_F = 45 deg, β_R = 44 deg, J = 2.0, HS3155).

case is 8% of blade tip diameter. The sectional thrust at three-quarters tip radius, as computed from a quasisteady approximation, is shown in Fig. 11, for the front blade, and Fig. 12, for the rear blade. The quasisteady model assumes uniform axial wake doublet strength. The wake doublet strength adjusts instantaneously to a new value at each new time step as if it were independent of the loading history. The abscissa represents two blade passing periods. The shape and phasing of the load histories on the front and rear blade are basically the same for the two methods. However, the present method predicted about 12% more thrust at that radial location. The significance of this comparison is that when the present scheme is run in quasisteady mode (with no spanwise vortex shedding and with the time derivative in Bernoulli's equation dropped), the two methods should give the same answer, apart from thickness effects and discretization errors. In fact, the present results use more chordwise panels but fewer spanwise panels. One similar trend for the two predicted results is that both methods show larger fluctuation on the fore rotor. This reason for larger fore rotor unsteady loading is simply because the fore rotor is 'near' highly loaded leading edge of the rear rotor, but the rear is near lightly loaded trailing edge of the fore rotor. The time-averaged overall thrust coefficient in Fig. 13, overall power coefficient in Fig. 14, and power coefficient for individual rotors in Fig. 15 indicate the present method agrees very well with both experimental results[16] and the vortex lattice method.[9]

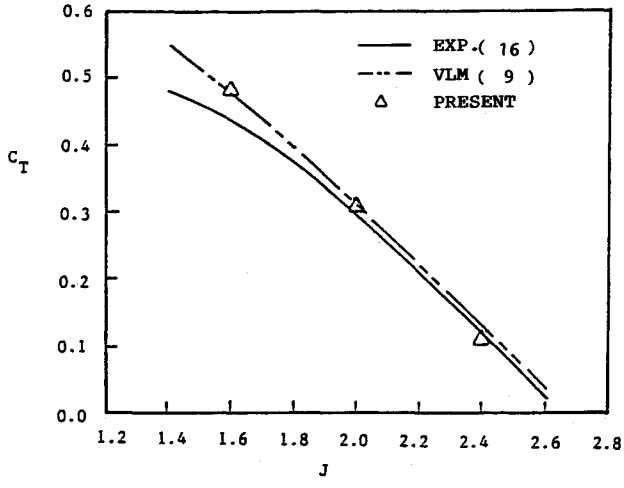

Fig. 13 Comparison of predicted and measured thrust (β_F = 45 deg, β_R = 44 deg, N_B = 4 × 4, HS3155).

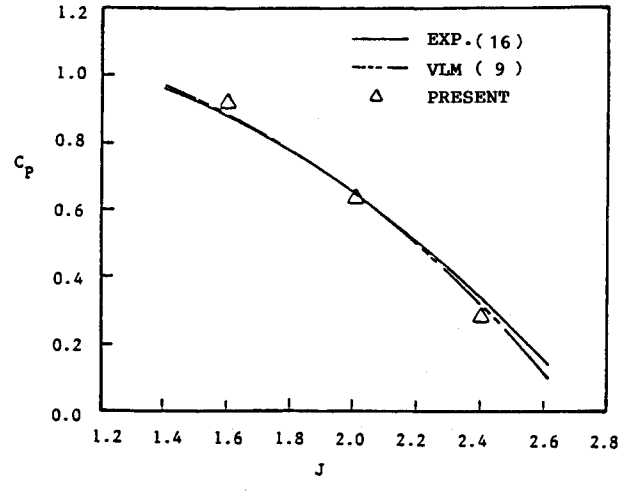

Fig. 14 Comparison of predicted and measured power (β_F = 45 deg, β_R = 44 deg, N_B = 4 × 4, HS3155).

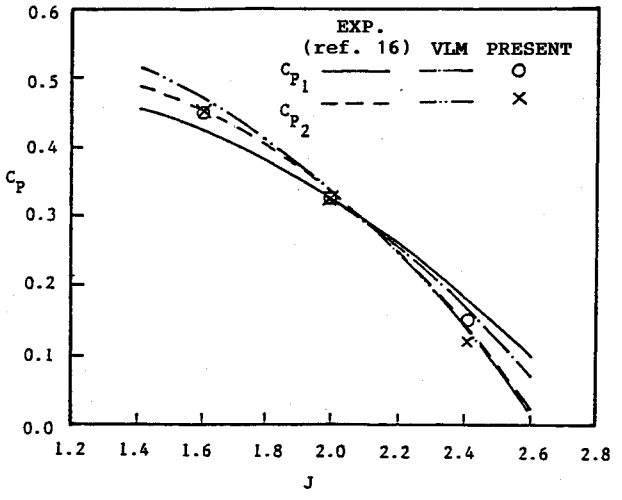

Fig. 15 Comparison of predicted and measured individual power (β_F = 45 deg, β_R = 44 deg, N_B = 4 × 4, HS3155).

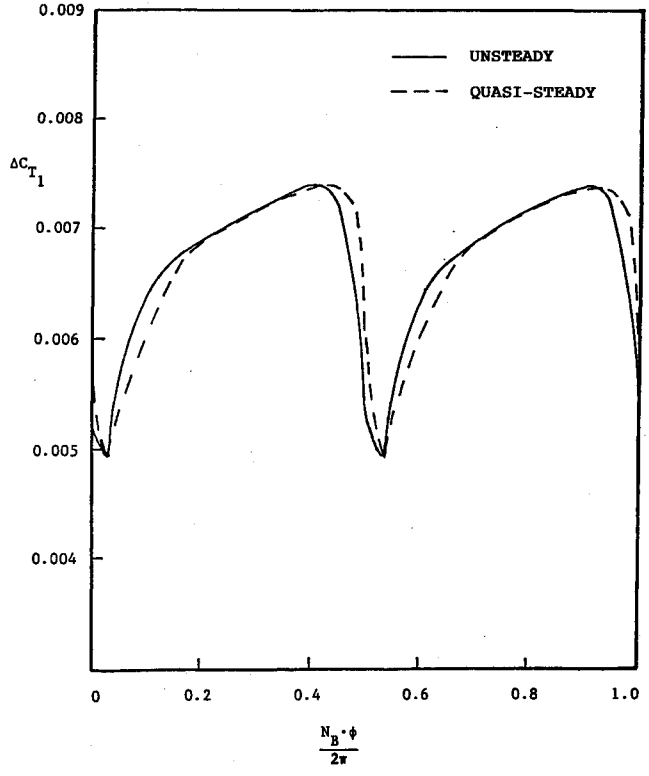

Fig. 16 Unsteady elemental thrust on front rotor (r/r_{tip} = 0.75, N_B = 4 × 4, β_F = 45 deg, β_R = 44 deg, J = 2.0, HS3155).

We now examine the results of fully unsteady calculations in comparison to quasisteady results. The unsteady analysis uses axially periodically varying vorticities. The wake doublet depends on the potential distribution on the blade surface. Once it is generated, it is convected downstream without change in strength. For the HS3155 rotor at the same operating condition as in Fig. 16, the unsteady terms at three-quarters tip radius produce little change in the load on the forward blade, as might be expected from the long interaction wavelength in the case (about four chords). However, on the rear rotor the fluctuating amplitude is considerably larger than in the quasisteady calculation, as shown in Fig. 17. This must be due to the blade-wake interaction. Figures 18 and 19 show the comparison of quasisteady and unsteady loads for the SR2 rotor, with same angle setting 41.34 deg at three-quarters tip radius fore and aft rotors, and Figs. 20 and 21 show the power. Here

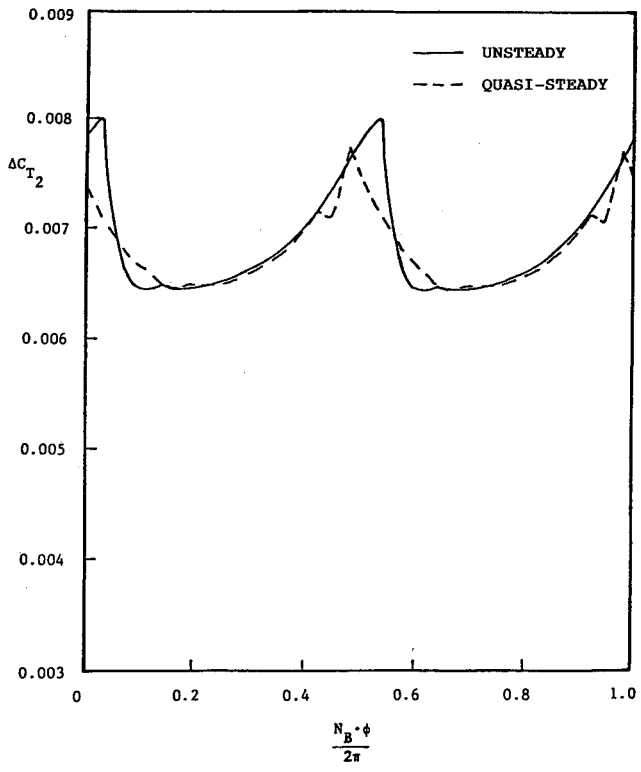

Fig. 17 Unsteady elemental thrust on rear rotor (r/r_{tip} = 0.75, N_B = 4 × 4, β_F = 45 deg, β_R = 44 deg, J = 2.0, HS3155).

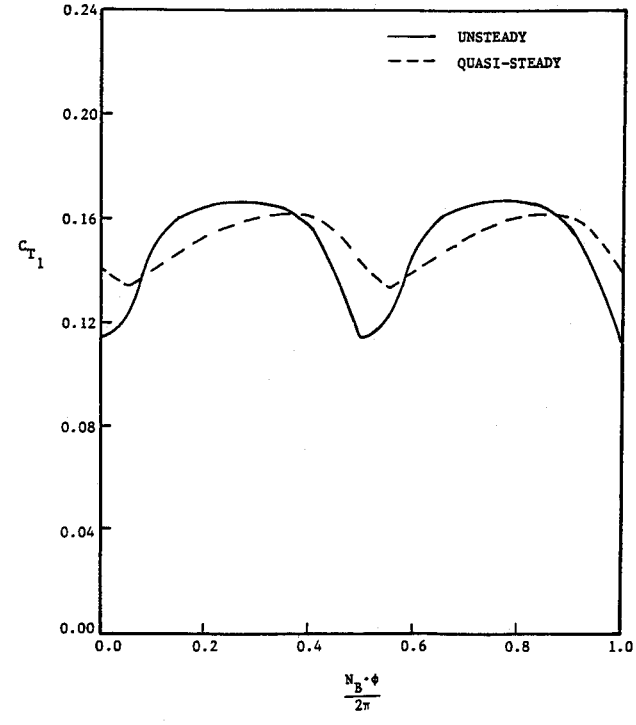

Fig. 18 Unsteady total thrust on front rotor ($\beta_{3/4}$ = 41.34 deg, N_B = 4 × 4, J = 1.633, SR2).

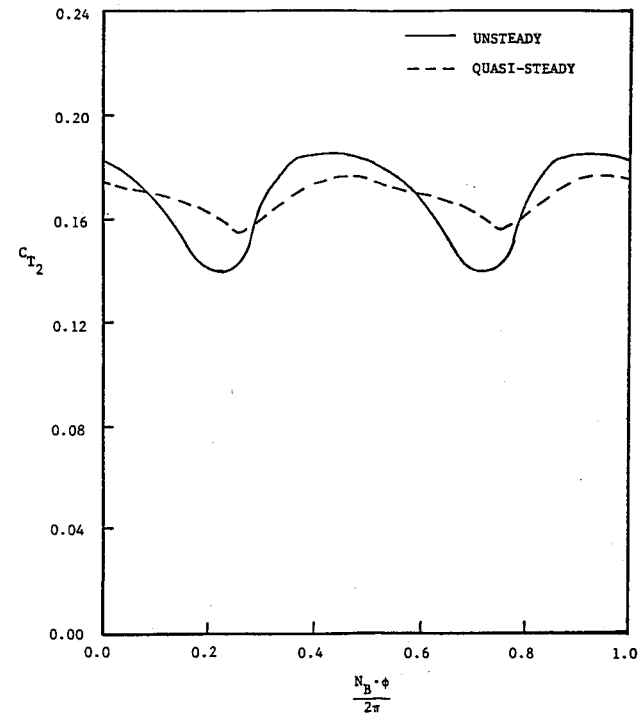

Fig. 19 Unsteady total thrust on rear rotor ($\beta_{3/4}$ = 41.34 deg, N_B = 4 × 4, J = 1.633, SR2).

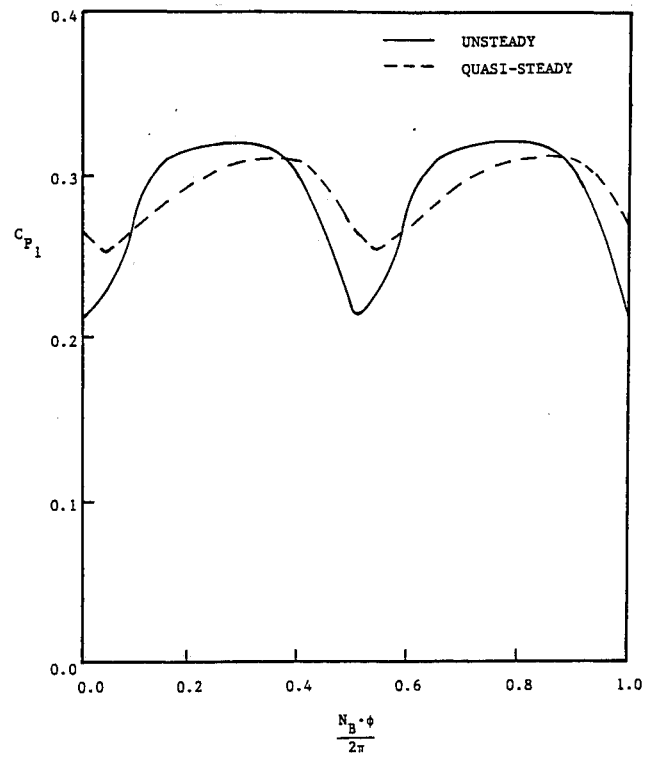

Fig. 20 Unsteady total power on front rotor ($\beta_{3/4}$ = 41.34 deg, N_B = 4 × 4, J = 1.633, SR2).

the unsteady amplitude is significantly larger on both rotors. In comparison to the HS3155, the SR2 has a larger reduced frequency (about 2.3) and a shorter wavelength (about 1.3 chords) because of its smaller aspect ratio. The mean loading on the rear rotor is significantly larger than that on the fore rotor. This is because the rear rotor experiences higher pressure and higher velocity inflow. In addition, the efficiency on the rear rotor is higher (about 1%) than that of the fore rotor. This is because the rear rotor recovers part of the swirl energy generated by the fore rotor.

Figures 22 and 23 contain comparisons of the present unsteady results to those obtained by Lesieutre. Besides the difference of time-averaged value for the two methods (which was apparent in the quasisteady results), there is a substantial difference between the two: the present scheme shows an increase in amplitude over quasisteady, whereas Lesieutre's

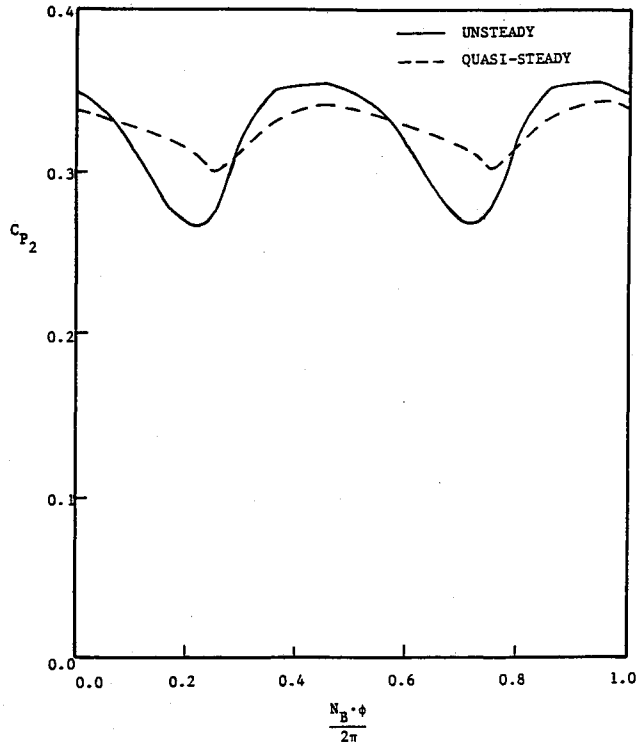

Fig. 21 Unsteady total power on rear rotor ($\beta_{3/4}$ = 41.34 deg, N_B = 4 × 4, J = 1.633, SR2).

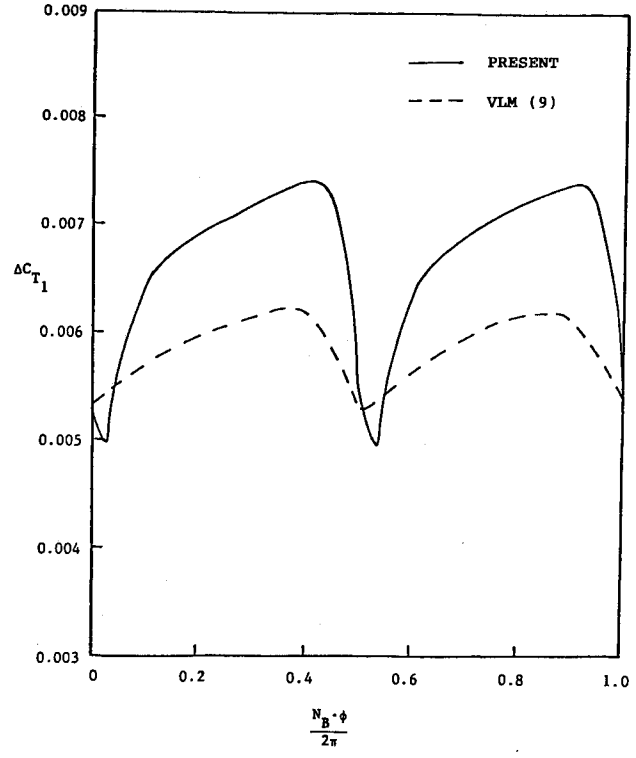

Fig. 22 Unsteady elemental thrust on front rotor; a comparison between present method and vortex lattice method (r/r_{tip} = 0.75, N_B = 4 × 4, β_F = 45 deg, β_R = 44 deg, J = 2, HS3155).

results show a decrease. That the latter method should show a decrease is obvious: the unsteady response is simply the quasisteady response harmonically decomposed, filtered by the Sears function, and reconstituted. Since the Sears function is less than one in magnitude at all frequencies, the end product is a net decrease in amplitude. However, the Sears function is, of course, a two-dimensional transfer function and so

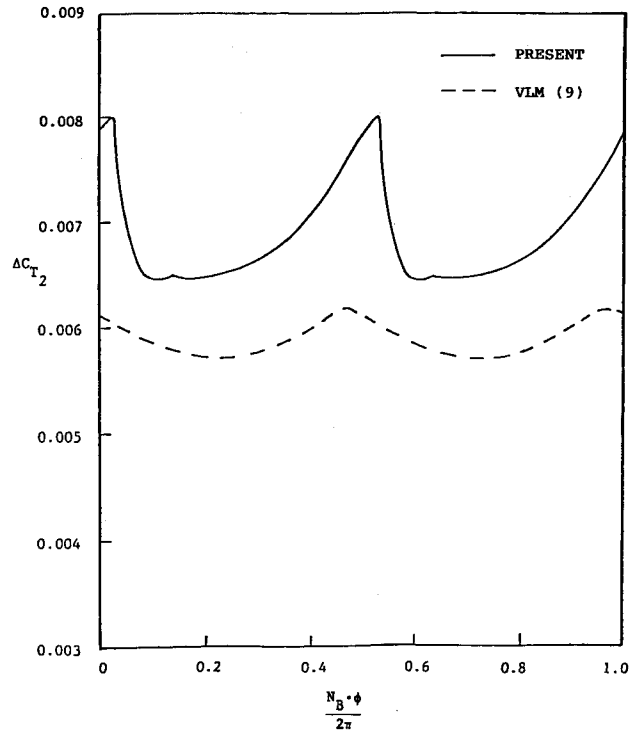

Fig. 23 Unsteady elemental thrust on rear rotor; a comparison between present method and vortex lattice method (r/r_{tip} = 0.75, N_B = 4 × 4, β_F = 45 deg, β_R = 44 deg, J = 2, HS3155).

can only be a rough approximation. It should be correct at zero frequency and for very high harmonics (with wavelengths short compared to the span) but may well be qualitatively wrong at intermediate frequencies.

The present unsteady results show sharp changes in loading twice per passing period. These can be correlated with blade relative position. The sudden drop in load on the front rotor, and rise on the aft, occur when the aft blade is immediately behind the front (minimum separation). The sudden rise on the front blade and drop on the rear occurs when the rear blade passes through a wake. The slope of the curves are smaller at the other locations for the relative position between blades, and wakes are larger, hence the blade-blade and blade-wake interactions are smaller. Therefore, the distinctive features of the unsteady response do have an apparent and reasonable cause.

Conclusions

The Green's function-based panel method decribed here is capable of computing time-dependent incompressible irrotational flows for single-rotation and counter-rotation propellers. For the single-rotation cases examined, our results were in good agreement with both lifting surface theory and experimental performance data (though the present method is more expensive than lifting surface theory and so has no distinct advantage in single-rotation applications). For the counter-rotation cases, a low aspect ratio propfan blade SR2 and a high aspect ratio classical propeller HS3155 were examined. The quasisteady results are in reasonable agreement with those of Lesieutre. The mean value of the quasisteady result is the same as that of unsteady calculation. The comparison of the mean values with experimental performance results and vortex lattice method showed very good agreement. However, the strip theory corrections that Lesieutre made do not appear to correlate at all well with our unsteady results. The present calculations for both configurations, SR2 and HS3155, show that the unsteady analysis predicted larger unsteady fluctuations than that of quasisteady analysis. The difference between the two predictions is a function of re-

duced frequency: the higher the reduced frequency, the more deviation of unsteady loading from the quasisteady loading.

The method should be a useful tool not only for performance estimates but also for aeroelastic and aeroacoustic applications to counter-rotation configurations and prop-wing interaction studies, particularly if the scheme can be extended to higher Mach numbers.

Acknowledgments

The work reported here has been supported by NASA Lewis Research Center under Grant No. 3-499 with Dr. K. R. V. Kaza as the grant monitor. The authors would also like to thank Dr. K. Tseng of United Technologies Research Center for his valuable discussions and suggestions.

References

[1]Dunham, D. M., Gentry, G. L., Jr., and Coe, P. L., Jr., "Low Speed Wind-Tunnel Tests of Single and Counter Rotation Propellers," NASA TM 87656, April 1986.

[2]Mitchell, G. A., and Mikkelson, D. C., "Summary and Recent Results from the NASA Advanced High-Speed Propeller Research Program," NASA TM 82891, June 1982.

[3]Lock, C. N. H., "Interference Velocity for a Close Pair of Contra-Rotating Airscrews," ARC RM No. 2084, July 1941.

[4]Theodorsen, T., *Theory of Propellers*, McGraw-Hill, New York, 1948.

[5]Celestina, M. L., Mulac, R. A., and Adamczyk, J. J., "A Numerical Simulation of the Inviscid Flow Through a Counter-Rotating Propeller," American Society of Mechanical Engineers, New York, ASME Paper 86-GT-138, J. of Turbomachinery, Transactions of the ASME, Vol. 108, No. 4, p. 187–193, Oct. 1986.

[6]Colehour, J. L., Davenport, F. J., and Sokhey, J. S., "Analysis of Counter Rotating Propeller Performance," AIAA Paper 85-005, Jan. 1985.

[7]Whitfield, D. L., Swafford, T. W., Janus, J. M., Mulac, R. A., and Belk, D. M., "Three-Dimensional Unsteady Euler Solution for Propfans and Counter-Rotating Propfans in Transonic Flow," AIAA Paper 87-1197, June 1987.

[8]Lesieutre, D. J., and Sullivan, J. P., "The Analysis of Counter-Rotating Propeller Systems," Society of Automotive Engineers, Warrendale, PA, SAE Paper 850869, April 1985.

[9]Lesieutre, D. J., and Sullivan, J. P., "Unsteady Forces on Counter-Rotating Propeller Blades," AIAA Paper no. 86-1804, June 1986.

[10]Chen, L. T., Suciu, E. O., and Morino, L., "A Finite Element Method for Potential Aerodynamics around Complex Configurations," AIAA Paper 74-107, Jan. 1974.

[11]Hunt, B., "Recent and Anticipated Advances in the Panel Method: The Key to Generalized Field Calculations," von Karman Institute lecture series, 1980-5, Belgium, 1980.

[12]Margason, R. J., Kjelgarrd, S. D., Sellers, W. L., III, Morris, C. E. K., Jr., Walkey, K. B., and Shields, E. W., "Subsonic Panel Methods—A Comparison of Several Production Codes," AIAA Paper 85-0280, Jan. 1985.

[13]Morino, L., "A General Theory of Unsteady Compressible Potential Aerodynamics," NASA CR-2464, Dec. 1974.

[14]Williams, M. H., and Hwang, C. C., "Three Dimensional Unsteady Aerodynamic and Aeroelastic Response of Advanced Turboprops," AIAA Paper 86-0846, May 1986.

[15]Biermann, D., and Hartman, E. P., "Wind Tunnel Tests of Four- and Six-Blade Single and Dual Rotating Tractor Propellers," NACA Report 747, July 1942.

[16]Biermann, D., and Gray, W. H., "Wind Tunnel Tests of Single- and Dual-Rotating Propellers Having from Three to Eight Blades," NACA Wartime Report L-359, Feb. 1942.